Received: 15 July 2019 | Revised: 24 September 2019 | Accepted: 28 October 2019

DOI: 10.4218/etrij.2019-0343

ORIGINAL ARTICLE

ETRI Journal WILEY

Signal parameter estimation through hierarchical conjugate gradient least squares applied to tensor decomposition

Long Liu | **Ling Wang** | **Jian Xie** | **Yuexian Wang** | **Zhaolin Zhang**

School of Electronics and Information, Northwestern Polytechnical University, Xi'an, China

Correspondence
Long Liu, School of Electronics and Information, Northwestern Polytechnical University, Xi'an, China.
Email: liulongnwpu@126.com

Funding information
National Natural Science Foundation of China, Grant/Award Number: 61601372 and 61771404

A hierarchical iterative algorithm for the canonical polyadic decomposition (CPD) of tensors is proposed by improving the traditional conjugate gradient least squares (CGLS) method. Methods based on algebraic operations are investigated with the objective of estimating the direction of arrival (DoA) and polarization parameters of signals impinging on an array with electromagnetic (EM) vector-sensors. The proposed algorithm adopts a hierarchical iterative strategy, which enables the algorithm to obtain a fast recovery for the highly collinear factor matrix. Moreover, considering the same accuracy threshold, the proposed algorithm can achieve faster convergence compared with the alternating least squares (ALS) algorithm wherein the highly collinear factor matrix is absent. The results reveal that the proposed algorithm can achieve better performance under the condition of fewer snapshots, compared with the ALS-based algorithm and the algorithm based on generalized eigenvalue decomposition (GEVD). Furthermore, with regard to an array with a small number of sensors, the observed advantage in estimating the DoA and polarization parameters of the signal is notable.

KEYWORDS

canonical polyadic decomposition, direction of arrival, factor matrix, hierarchical conjugate gradient least squares, polarization parameters

1 | INTRODUCTION

Over the past few decades, signal parameter estimation has been widely applied to various fields, such as sonar, radar, seismic exploration, wireless communications, and so on. Moreover, signal parameter estimation is an extensively investigated subject in the field of array signal processing. According to previous practical and academic studies, there are two types of signal parameters that are of great significance and should not be overlooked. The first type refers to all spatial parameters, such as the direction of arrival (DoA), while the second type consists of all polarization parameters, such as the auxiliary angle and polarization phase difference. To achieve better performance in estimating these signal parameters, many parameter estimation algorithms have been proposed thus far. For example, algorithms based on the vector-arr.ay, which mainly adopt eigenspace-based techniques, have a long history. Most of these methods, such as multiple signal classification (MUSIC) [1], estimation of signal parameters using rotational invariance techniques (ESPRIT) [2], and their derivatives [3,4], share a common feature whereby the estimation process is based on two-dimensional matrix operations. Additionally, researchers have recently

developed more advanced algorithms based on the scalar-array, wherein most signal models and measured data are based on matrix operations [5–8]. The dual-frequency signal model proposed in [5] is an excellent example of such techniques.

Apart from the abovementioned algorithms, the last few years have also witnessed the growing popularity of tensor operations in the field of signal processing owing to their advantage of being inherently multidimensional. Previous studies [9–11] introduced the technique of array beamforming, which is based on the decomposition of multidimensional signal tensor models. For example, in [11], methods using tensor operations were investigated to improve the robustness of array beamforming. Therein, a tensor decomposition method, which is mainly used to construct a distortionless response model with a minimum variance, was incorporated into the improved conjugate gradient least squares (CGLS) method to achieve better robustness. Additionally, researchers have also devoted considerable attention to the canonical polyadic decomposition (CPD) of third-order tensors. This subject has been widely investigated in the field of mathematics [12–15], and remarkable contributions to the application of signal separation have also been made [16–21]. For example, in [20], a method of DoA estimation for seismic plane waves was considered from a deterministic viewpoint using CPD, and the different propagation speed of waves was also considered using the tensor's multidimensional feature, in addition to temporal and spatial information. Likewise, [21] also proposed a CPD-based approach using generalized eigenvalue decomposition (GEVD) to achieve time-delay estimation for a tensor-based GNSS receiver. From the above review, it follows that tensor operations have become very popular in the field of signal processing.

Notably, recent studies have provided strong evidence for the excellent convergence characteristics of the CGLS algorithm and the conjugate gradient (CG) algorithm in signal processing [22–25]. Moreover, we cannot ignore the prevalence of least squares (LS) algorithms and stochastic gradient (SG) algorithms in the field of parameter estimation [26–28]. To improve the accuracy of parameter estimation, iterative algorithms [29–33] based on hierarchical concepts have also been extensively investigated. For example, in [29], a hierarchical multi-innovation stochastic gradient estimation algorithm was derived using parameter decomposition.

Based on a comprehensive review of the abovementioned literature, the objective of this study was to investigate the CPD of a third-order tensor data model by improving the CGLS algorithm and then estimating the signal parameters. Specifically, we investigated the application of CGLS to the tensor CPD, and combined the data model to propose a hierarchical CGLS-based algorithm for the CPD (HCGLS-CPD). Moreover, we analyzed the GEVD-based algorithm for CPD (GEVD-CPD) and the CPD algorithm based on the alternating least squares (ALS-CPD) for comparison with the proposed HCGLS-CPD algorithm. Note that the proposed algorithm does not only focus on DoA estimation but also on the estimation of the polarization parameters delivered by the signal. The strength of our algorithm lies in its excellent performance compared with the GEVD-CPD, ALS-CPD, and HALS-CPD algorithms when shorter snapshots are provided and the array has a small number of sensors.

The rest of this paper is organized as follows. The derivation of the tensor-based data model is presented in Section 2. The GEVD-CPD and ALS-CPD algorithms are reviewed in Section 3. The development of the HCGLS-CPD algorithm and the algebraic operations for extracting the signal parameters are presented in Section 4. Moreover, the numerical simulations are presented in Section 5. Finally, the conclusions drawn from this study are presented in the final section. The algebraic notations used in the paper are presented in Table 1.

2 | DATA MODEL

Let us consider a vector-array composed of L EM vector-sensors located at $\mathbf{h}_l \in \mathbb{R}^3$ for $l = 1, \ldots, L$; the number of the component measured by an EM vector-sensor is J. It is assumed that R signals with the complex amplitudes of $\{s_r(k), r = 1, \ldots, R\}$ impinge on the array from the directions $\{-\varepsilon_r, r = 1, \ldots, R\}$, where $\varepsilon_r = -[\sin\phi_r \cos\theta_r \ \sin\phi_r \sin\theta_r \ \cos\phi_r]^T, \theta_r \in [0, 2\pi]$ denotes the azimuth angle, and $\phi_r \in [0, \pi]$ denotes the elevation angle. The spatial steering vector of the signal with DoA (θ, ϕ) is expressed as follows:

$$\mathbf{a}^s(\theta, \phi) = [e^{-i2\pi(\mathbf{h}_1^T \varepsilon/\lambda)}, \ldots, e^{-i2\pi(\mathbf{h}_L^T \varepsilon/\lambda)}]^T. \quad (1)$$

TABLE 1 Algebraic notations

υ	Scalar υ
$\mathbf{v}$	Scalar $\mathbf{v}$
$\mathbf{A}$	Matrix $\mathbf{A}$
$\mathcal{A}$	Tensor $\mathcal{A}$
$\mathbb{R}$	Real number field
$\mathbb{C}$	Complex number field
$\mathbf{A}^T$	Transpose of $\mathbf{A}$
$\mathbf{A}^H$	Conjugate transpose of $\mathbf{A}$
$\mathcal{A} \odot \mathcal{B}$	Outer product between $\mathcal{A}$ and $\mathcal{B}$
$\mathbf{A} \otimes \mathbf{B}$	Kronecker product between $\mathbf{A}$ and $\mathbf{B}$
$\mathbf{A} \odot \mathbf{B}$	Khatri-Rao product between $\mathbf{A}$ and $\mathbf{B}$
$\mathbf{A} \circ \mathbf{B}$	Hadamard product between $\mathbf{A}$ and $\mathbf{B}$
$r_{\mathbf{A}}$	Rank of matrix $\mathbf{A}$
$\|\mathbf{A}\|_F$	Frobenius norm of $\mathbf{A}$
$\|\mathbf{v}\|_2$	2-norm of $\mathbf{v}$

The polarization steering vector of the signal with the spatial-polarization parameter $\Psi=(\theta,\phi,\gamma,\eta)$ is expressed as follows:

$$\mathbf{a}^{p}(\Psi)=\mathfrak{B}\underbrace{\begin{bmatrix}-\sin\theta & \cos\phi\cos\theta\\ \cos\theta & \cos\phi\sin\theta\\ 0 & -\sin\phi\\ \cos\phi\cos\theta & \sin\theta\\ \cos\phi\sin\theta & -\cos\theta\\ -\sin\phi & 0\end{bmatrix}}_{\Xi_{\theta,\phi}}\underbrace{\begin{bmatrix}\cos\gamma\\ \sin\gamma e^{i\eta}\end{bmatrix}}_{\mathbf{h}_{\gamma,\eta}} \tag{2}$$

where $\gamma\in[0,\pi/2]$ and $\eta\in[-\pi,\pi]$ denote the polarization auxiliary angle and the polarization phase difference, respectively. $\mathfrak{B}\in\mathbb{R}^{J\times 6}$ denotes the polarization selection matrix of the EM vector-sensor. Particularly, $\mathfrak{B}=[\mathbf{I}_{3\times3},\mathbf{0}_{3\times3}]$ represents the polarization selection matrix of the three-dipoles, and $\mathfrak{B}=\mathbf{I}_{6\times6}$ belongs to the complete EM vector-sensor, where $\mathbf{I}$ denotes the identity matrix. The spatial-polarization steering vector can be further expressed as follows:

$$\mathbf{a}(\Psi)=\mathbf{a}^{s}(\theta,\phi)\otimes\mathbf{a}^{p}(\Psi). \tag{3}$$

Therefore, the vector-output of the array at instant t_k can be modeled as follows:

$$\boldsymbol{x}(k)=\sum_{r=1}^{R}\mathbf{a}(\Psi_r)s_r(k)+\mathbf{n}(k), \tag{4}$$

where $\mathbf{n}(k)$, which is an additive and Gaussian complex circular, denotes the spatial prewhitening noise.

Considering that the multidimensional nature of the tensor only caters to the multi-domain nature of the signal, the following spatial-polarization steering tensor can be obtained by performing tensorization on (3), as follows:

$$\mathcal{A}(\Psi)=\mathbf{a}^{p}(\Psi)\circledcirc\mathbf{a}^{s}(\theta,\phi). \tag{5}$$

Moreover, because the consecutive K snapshots can be written as $\mathbf{s}=[s(1),\ldots,s(K)]$, the tensor-output of K snapshots can be expressed as follows:

$$\begin{aligned}\mathcal{X}&=\sum_{r=1}^{R}A(\Psi_r)\circledcirc\mathbf{s}_r+\mathcal{N}\\ &=\sum_{r=1}^{R}\mathbf{a}^{p}(\Psi_r)\circledcirc\mathbf{a}^{s}(\theta_r,\phi_r)\circledcirc\mathbf{s}_r+\mathcal{N}\end{aligned}, \tag{6}$$

where $\mathcal{X}\in\mathbb{C}^{J\times L\times K}$ and $\mathcal{N}\in\mathbb{C}^{J\times L\times K}$ represent the tensor noise subject to the tensorization regarding the noise matrix $\mathbf{N}=[\mathbf{n}(1),\ldots,\mathbf{n}(k)]$.

3 | GEVD-CPD AND ALS-CPD FOR DATA MODEL

Let $\mathcal{T}=\sum_r^R\mathbf{a}_r\circledcirc\mathbf{b}_r\circledcirc\mathbf{c}_r$, where $\mathbf{a}_r\in\mathbb{C}^J$, $\mathbf{b}_r\in\mathbb{C}^L$, and $\mathbf{c}_r\in\mathbb{C}^K$ are the scaled representations of $\mathbf{a}^{p}(\Psi_r)$, $\mathbf{a}^{s}(\theta_r,\phi_r)$, and $\mathbf{s}_r$, respectively; that is, $\mathbf{a}_r=a[\mathbf{a}^{p}(\Psi_r)]$, $\mathbf{b}_r=b[\mathbf{a}^{s}(\theta_r,\phi_r)]$, $\mathbf{c}_r=c[\mathbf{s}_r]$, and $abc=1$. Therefore, (6) can be expressed as follows:

$$\mathcal{X}=\mathcal{T}+\mathcal{N}. \tag{7}$$

Moreover, we can also write $\mathcal{T}$ as follows: $\mathcal{T}=[\mathbf{A},\mathbf{B},\mathbf{C}]_R$, where $\mathbf{A}=[\mathbf{a}_1,\ldots,\mathbf{a}_R]\in\mathbb{C}^{J\times R}$, $\mathbf{B}=[\mathbf{b}_1,\ldots,\mathbf{b}_R]\in\mathbb{C}^{L\times R}$, and $\mathbf{C}=[\mathbf{c}_1,\ldots,\mathbf{c}_R]\in\mathbb{C}^{K\times R}$ are the first, second, and third factor matrix of $\mathcal{T}$, respectively.

Note that in (7), $\mathcal{N}$ is an unknown noise tensor and $\mathcal{X}$ is the given tensor. Generally, the factor matrices of $\mathcal{T}$ are approximated by the solution of the optimization problem

$$\min\|\mathcal{X}-[\mathbf{A},\mathbf{B},\mathbf{C}]_R\|, \tag{8}$$

where $\|\cdot\|$ denotes a suitable norm [14].

3.1 | GEVD-CPD algorithm

Herein, we first reshape $\mathcal{T}$ into a matrix $\mathbf{T}_{(1)}\in\mathbb{C}^{JL\times K}$ as follows: the (j,l,k)th entry of $\mathcal{T}$ corresponds to the $((j-1)L+l,k)$th entry of $\mathrm{T}_{(1)}$. Specifically, the rank-1 tensor $\mathbf{a}_r\circledcirc\mathbf{b}_r\circledcirc\mathbf{c}_r$ corresponds to the rank-1 matrix $(\mathbf{a}_r\otimes\mathbf{b}_r)\mathbf{c}_r^T$ [15]. Thus, the matrix unfolding of (6) can be identified with

$$\mathbf{T}_{(1)}=\begin{bmatrix}\mathbf{T}_1\\ \vdots\\ \mathbf{T}_J\end{bmatrix}=\begin{bmatrix}\mathbf{B}\mathrm{Diag}(\mathbf{a}^1)\mathbf{C}^T\\ \vdots\\ \mathbf{B}\mathrm{Diag}(\mathbf{a}^J)\mathbf{C}^T\end{bmatrix}=(\mathbf{A}\odot\mathbf{B})\mathbf{C}^T, \tag{9}$$

where $\mathbf{a}^j$ denotes the ith row of the matrix $\mathbf{A}$, $j=1,\ldots,J$. Similarly, we can reshape $\mathbf{a}_r\circledcirc\mathbf{b}_r\circledcirc\mathbf{c}_r$ into matrices $(\mathbf{b}_r\otimes\mathbf{c}_r)\mathbf{a}_r^T$ and $(\mathbf{c}_r\otimes\mathbf{a}_r)\mathbf{b}_r^T$, and obtain the following factorizations:

$$\mathbf{T}_{(2)}=(\mathbf{B}\odot\mathbf{C})\mathbf{A}^T,\quad \mathbf{T}_{(3)}=(\mathbf{C}\odot\mathbf{A})\mathbf{B}^T. \tag{10}$$

The core of the GEVD-CPD approach is the following straightforward connection between any two slices $\mathbf{T}_{j_1}$ and $\mathbf{T}_{j_2}$:

$$\mathbf{T}_{j_1}\mathbf{T}_{j_2}^{\dagger}=\mathbf{B}\mathrm{Diag}(\mathbf{a}^{j_1})\mathrm{Diag}(\mathbf{a}^{j_2})^{-1}\mathbf{B}^{\dagger}, \tag{11}$$

$$\mathbf{T}_{j_1}^T(\mathbf{T}_{j_2}^T)^{\dagger}=\mathbf{C}\mathrm{Diag}(\mathbf{a}^{j_1})\mathrm{Diag}(\mathbf{a}^{j_2})^{-1}\mathbf{C}^{\dagger}, \tag{12}$$

where $j_1,j_2=1,\ldots,J$, $j_1\neq j_2$, and $(\cdot)^{\dagger}$ denote the Moore-Penrose inverse. From (9), we consider the following relationship:

$\mathbf{T}_j = \mathbf{B}\text{Diag}(\mathbf{a}^j)\mathbf{C}^T$. Hence, for any j, $\text{Diag}(\mathbf{a}^j) = \mathbf{B}^\dagger \mathbf{T}_j (\mathbf{C}^T)^\dagger$. The CPD features are as follows:

1. The factor matrices **B** and **C** follow the GEVD of the matrix pencils $(\mathbf{T}_{j_1}, \mathbf{T}_{j_2})$ and $(\mathbf{T}_{j_1}^T, \mathbf{T}_{j_2}^T)$.
2. The rows of the factor matrix **A** can be recovered using the following relationship:$\text{Diag}(\mathbf{a}^j) = \mathbf{B}^\dagger \mathbf{T}_j (\mathbf{C}^T)^\dagger$.

Notably, the premise of the GEVD-CPD algorithm is that the factor matrices **A**, **B**, and **C** are full column rank. In particular, the known tensor $\mathcal{X}$ is used as an approximation of $\mathcal{T}$ because $\mathcal{T}$ is unknown.

3.2 | ALS-CPD algorithm

The optimization problem (8) can be solved by minimizing the Frobenius norm of the error given with the following form:

$$\min \| \mathcal{X} - \sum_{r}^{R} \mathbf{a}_r \circledcirc \mathbf{b}_r \circledcirc \mathbf{c}_r \|_F. \tag{13}$$

Considering the manner in which the factor matrix **C** is updated, the simplest method is to rewrite the objective function in quadratic form, as follows:

$$\min \| \mathbf{X}_{(1)}^T - \mathbf{C}(\mathbf{B} \odot \mathbf{A})^T \|_F, \tag{14}$$

where $\mathbf{X}_{(1)}$ is the matrix unfolding of tensor $\mathcal{X}$. Thus, the factor matrix **C** can be updated in closed form, as follows:

$$\mathbf{C} = \mathbf{X}_{(1)}^T (\mathbf{B} \odot \mathbf{A})((\mathbf{B}^T\mathbf{B}) \circ (\mathbf{A}^T\mathbf{A}))^{-1}. \tag{15}$$

Similarly, the updated methods of the factor matrices **A** and **B** can be derived. To obtain the optimal solution of the problem (13), it is necessary to update the matrices **A**, **B**, and **C** through multiple iterations, as described by Algorithm 1. The iteration is terminated when $\| e \|_F \leq \varepsilon$, where ε denotes the threshold defined by the users.

Algorithm 1 Procedure of ALS-CPD algorithm

Require: Initialize the matrices **A** and **B**.

1: **while** $e > \varepsilon$ do
2: for $n = 1$ to 3
3: case $n = 1$: $\mathbf{C} = \mathbf{X}_{(1)}^T (\mathbf{B} \odot \mathbf{A})((\mathbf{B}^T\mathbf{B}) \circ (\mathbf{A}^T\mathbf{A}))^{-1}$.
4: case $n = 2$: $\mathbf{A} = \mathbf{X}_{(2)}^T (\mathbf{C} \odot \mathbf{B})((\mathbf{C}^T\mathbf{C}) \circ (\mathbf{B}^T\mathbf{B}))^{-1}$.
5: case $n = 3$: $\mathbf{B} = \mathbf{X}_{(3)}^T (\mathbf{A} \odot \mathbf{C})((\mathbf{A}^T\mathbf{A}) \circ (\mathbf{C}^T\mathbf{C}))^{-1}$.
6: end for
7: $e = \| \mathbf{X}_{(1)}^T - \mathbf{C}(\mathbf{B} \odot \mathbf{A})^T \|_F \; / \; \| \mathbf{X}_{(1)}^T \|_F$
8: **end while**

Ensure: **A**, **B** and **C**.

4 | PROPOSED HIERARCHICAL CGLS-CPD ALGORITHM

The traditional CGLS algorithm is the mathematically equivalent form of the CG algorithm, when it is used to solve the LS problem $\min \| \boldsymbol{d} - \mathbf{M}\boldsymbol{w} \|$, where $\boldsymbol{d}$ and **M** represent the prior knowledge, and $\boldsymbol{w}$ is the parameter to be solved for. This section presents the HCGLS-CPD algorithm for the tensor-based data model.

4.1 | HCGLS-CPD algorithm

Considering the matrix unfolding form expressed by (9), the optimization problem expressed by (8) can be rewritten as follows:

$$\min \| \mathbf{X}_{(1)} - (\mathbf{A} \odot \mathbf{B})\mathbf{C}^T \|_F. \tag{16}$$

Equivalently, we can solve the problem (16) by optimizing the multiple sub-problems, as follows:

$$\min \| [\mathbf{X}_{(1)}]_{:,k} - \mathbf{M}\mathbf{c}^k \|_2, \quad k = 1, \ldots, K, \tag{17}$$

where $[\mathbf{X}_{(1)}]_{:,k}$ denotes the kth column of the matrix $\mathbf{X}_{(1)}$, and $\mathbf{c}^k$ denotes the kth row of the matrix **C**. In other words, the updated matrix **C** can be approximated as the global optimal solution of (16) by hierarchically solving the sub-optimization problem (17).

According to (8) and (10), the updated methods of matrices **A** and **B** can be obtained by the same token. Because it is important that matrices **A**, **B**, and **C** are unknown, hierarchical iteration must be carried out to bring the optimization result closer to the actual value.

The procedure of the proposed algorithm is summarized in Algorithm 2. First, the initializations of the unknown factor matrices **A**, **B**, and **C** are required. In this study, the initialization of matrices **A** and **B** can be achieved by setting any $\Psi = (\theta, \phi, \gamma, \eta)$ in (2) and (3). Any updated column of the arbitrary factor matrix can be obtained by the inner iteration in steps 6–16. This process is repeated until all columns of the factor matrix are updated. Then, the alternate updating of matrices **A**, **B**, and **C** is completed through the middle iteration in steps 2–18. Subsequently, it is determined whether the calculation accuracy described in step 1 is reached; if not, the updating of the factor matrices is continued; otherwise, the algorithm is terminated. The thresholds ε and ς in steps 1 and 6 are set by users strongly relying on their own experiences.

The obvious advantage of the proposed algorithm lies in its efficiency of handling factor matrices with highly collinear column vectors, owing to the adoption of a hierarchical optimization strategy. In other words, the proposed

algorithm independently optimizes the column vectors of each factor matrix, then iteratively updates each factor matrix, and thus effectively avoids the matrix inversion operation, which is an indispensable step for the ALS-CPD algorithm. Moreover, the updating of the factor matrix obviously tends to be ill-conditioned owing to the existence of matrix inversion operations in Algorithm 2, when any two of the three factor matrices have highly collinear column vectors.

Algorithm 2 Procedure of HCGLS-CPD algorithm

Require: Initialize matrices **A**, **B**, and **C**.
While $e > \varepsilon$ do {outer iteration}
For $q = 1$ to 3 {middle iteration}
Initialize: $\mathbf{M} = \mathbf{A} \odot \mathbf{B}$ or $\mathbf{B} \odot \mathbf{C}$ or $\mathbf{C} \odot \mathbf{A}$, corresponding to $q = 1$, $q = 2$, and $q = 3$, respectively; $N = K$ or J or L, when $q = 1$, $q = 2$, and $q = 3$, respectively; $\mathbf{D} = \mathbf{C}$ or $\mathbf{A}$ or $\mathbf{B}$, corresponding to $q = 1$, $q = 2$, and $q = 3$, respectively.
For $n = 1$ to N
Input: $\mathbf{w}_0 = \mathbf{d}^n$, $\mathbf{r}_0 = [\mathbf{X}_{(q)}]_{:,n} - \mathbf{M}\mathbf{w}_0$, $\mathbf{s}_0 = \mathbf{M}^H\mathbf{r}_0$, $\mathbf{p}_1 = \mathbf{s}_0$,$\zeta_0 = \| \mathbf{s}_0 \|_2^2$, $i = 0$
While $\| \mathbf{r}_i \|_2 > \varsigma$ do {inner iteration}
$i = i + 1$
$\mathbf{v}_i = \mathbf{M}^H\mathbf{p}_i$ //intermediate vector
$\alpha_i = \zeta_{i-1} / \| \mathbf{v}_i \|_2^2$
$\mathbf{w}_i = \mathbf{w}_{i-1} + \alpha_i\mathbf{p}_i$ //weight vector
$\mathbf{r}_i = \mathbf{r}_{i-1} - \alpha_i\mathbf{v}_i$ //LS residual
$\mathbf{s}_i = \mathbf{M}^H\mathbf{r}_i$ //intermediate vector
$\zeta_i = \| \mathbf{s}_i \|_2^2$
$\beta_{i+1} = \zeta_i / \zeta_{i-1}$
End while
$\mathbf{d}^n = \mathbf{w}_i$; that is, update the nth row in the corresponding factor matrix.
End for
End for
$e = \| \mathbf{X}_{(1)}^T - \mathbf{C}(\mathbf{B} \odot \mathbf{A})^T \|_F / \| \mathbf{X}_{(1)}^T \|_F$
End while
Ensure: **A**, **B** and **C**.

The derivation process of the ALS-CPD algorithm based on hierarchical theory is described in Appendix B. According to its iterative steps, it can be seen that its convergence performance is poor.

4.2 | Parameter estimation

From the abovementioned data model, it can be seen that the spatial-polarization parameters of the signals can be reflected by the factor matrix **A**, and factor matrix **B** only contains the spatial parameters of the signals. Therefore, once the factor matrices are obtained, the first step is to extract the spatial parameters from **B**.

4.2.1 | Estimation of spatial parameters

The spatial DoA of the rth signal impinging on the array can be estimated by solving the equations as follows:

$$\begin{cases} [\mathbf{b}_r]_1 = e^{-i2\pi(\mathbf{h}_1^T\varepsilon_r/\lambda),} \\ \vdots \\ [\mathbf{b}_r]_L = e^{-i2\pi(\mathbf{h}_L^T\varepsilon_r/\lambda)}. \end{cases} \tag{18}$$

The DoA (θ_r, ϕ_r) of the rth signal can be estimated from any two equations in (18). However, to improve the validity of the results, appropriate strategies can be formulated to obtain multiple sets of solutions from (18). Then, the average is calculated as the final solution.

4.2.2 | Estimation of polarization parameters

Once the DoA is estimated, the polarization parameters of the signals can be extracted from the factor matrix **A**. As mentioned above, $\mathbf{a}_r$ is the scaled representation of $\mathbf{a}^{\mathrm{p}}(\Psi_r)$, that is, $\mathbf{a}_r = a[\mathbf{a}^{\mathrm{p}}(\Psi_r)]$ and a is a scaling factor. Hence, according to (2), the polarization parameters (γ_r, η_r) of the rth signal can be obtained as follows:

$$\mathbf{a}_r = a\mathfrak{B}\Xi_{\theta_r,\phi_r}[\cos\gamma_r, \sin\gamma_r e^{i\eta_r}]^T. \tag{19}$$

5 | SIMULATIONS

This section discusses the numerical simulations conducted to demonstrate the efficiency of the proposed algorithm. We considered the following scenario using a uniform linear array (ULA) with complete EM vector-sensors and half wavelength spacing. Two signals impinged on the ULA from $(\theta_1, \phi_1) = (50°, 90°)$ and $(\theta_2, \phi_2) = (120°, 90°)$ with the polarization parameters $(\gamma_1, \eta_1) = (10°, 90°)$ and $(\gamma_2, \eta_2) = (30°, 90°)$, respectively. The noise component was assumed to be the zero-mean additive white Gaussian noise.

Throughout all simulations, the results were averaged by 200 Monte Carlo trials, and compared with the Cramér-Rao lower bound (CRB) benchmark, which is described in Appendix A. The performances of the GEVD-CPD algorithm, ALS-CPD algorithm, and HALS-CPD algorithm were also evaluated for comparison with the results obtained by the proposed algorithm. Additionally, the root mean square error (RMSE) involved in the simulations was calculated by

$$\mathrm{RMSE}(\mu)=\sqrt{\frac{1}{NR}\sum_{n=1}^{N}\sum_{r=1}^{R}(\hat{\mu}_{rn}-\mu_r)^2}, \tag{20}$$

where μ_r denotes one of parameters $\{\theta_r, \phi_r, \gamma_r, \eta_r\}$, and belongs to the rth signal; $\hat{\mu}_{rn}$ is the estimation of μ_r in the nth trial.

5.1 | Comparison of computational efficiency

The computational efficiency of the proposed algorithm was compared with that of three traditional algorithms (GEVD-CPD, ALS-CPD, and HALS-CPD) by recording the computational time of CPD under the various situations presented in Tables 2 and 3. We implemented the abovementioned algorithms in Matlab 2016a, and conducted an experiment using a personal computer with Intel Core i5 CPU6200U 2.3 GHz and 8 GB of memory on Windows 10. The ALS-CPD, HALS-CPD, and proposed algorithms used the relative error $e=\|\mathbf{X}_{(1)}^{T}-\mathbf{C}(\mathbf{B}\odot\mathbf{A})^{T}\|_F/\|\mathbf{X}_{(1)}^{T}\|_F$ as a stop criterion. The iterative processes of ALS-CPD, HALS-CPD, and HCGLS-CPD was terminated when the relative errors were lower than 0.5.

The number of sensors L was assumed as 4. In addition to the two abovementioned signals, another signal impinging on the ULA from $(\theta_3, \phi_3)=(30°, 90°)$ with the polarization parameters $(\gamma_3, \eta_3)=(60°, 90°)$ was considered to obtain the data presented in Table 3. As can be clearly seen, the proposed HCGLS-CPD algorithm achieved the highest computational efficiency in most test cases, although in a few cases its performance was occasionally weaker than that of the GEVD-CPD algorithm.

TABLE 2 Computational time (s) for different SNR and snapshots in case of $R = 2$

	30 dB		60 dB	
(SNR, K)	$K = 128$	$K = 512$	$K = 128$	$K = 512$
GEVD-CPD	0.487	1.157	0.450	1.163
ALS-CPD	0.632	0.856	0.639	0.778
HALS-CPD	10.26	16.81	11.01	15.63
HCGLS-CPD	0.471	0.557	0.479	0.572

TABLE 3 Computational time (s) for different SNR and snapshots in case of $R = 3$

	30 dB		60 dB	
(SNR, K)	$K = 128$	$K = 512$	$K = 128$	$K = 512$
GEVD-CPD	0.535	1.338	0.484	1.263
ALS-CPD	1.036	1.182	1.109	1.168
HALS-CPD	13.25	18.92	13.60	19.87
HCGLS-CPD	0.493	0.606	0.487	0.617

5.2 | Performance of proposed algorithm

It was assumed that the ULA consisted of four complete EM vector-sensors, and that SNR was 30 dB. The results presented in Figure 1 reveal that the proposed HCGLS-CPD algorithm had superior performance compared with the GEVD-CPD, ALS-CPD, and HALS-CPD algorithms when the number of snapshots was less than 250. As the number of snapshots increased, the performance of the HCGLS-CPD and GEVD-CPD algorithms tended to be similar. Additionally, particular attention should be paid to the ALS-CPD algorithm because its performance was inferior to that of the other three algorithms in most test cases, particularly when the number of snapshots was greater than 50.

Figure 2 presents the results of the scenarios wherein two different sensor numbers (L = 4, 8) were considered, both of which were tested against SNR for the fixed number of snapshots of K = 200. As can be clearly seen in Figure 2, the HCGLS-CPD algorithm outperformed the other three algorithms in each case wherein the SNR was greater than 25 dB, and had the fastest convergence speed even though its performance was not optimal in a few cases. However, as the number of sensors increased, the ALS-CPD algorithm gained an advantage whereby the accuracy of the DoA estimation markedly improved; the other three algorithms only achieved slight improvement.

Once the DoA was estimated as described in the above example, the polarization parameters could be estimated. Figure 3 shows the accuracy of the algorithms for parameter η in the same scenarios as Figure 2. As can be seen in the figure, the estimation accuracy of parameter η was lower than that of DoA for all algorithms, even though the performance differences amongst the algorithms were similar to the tendencies shown in Figure 2. This loss can

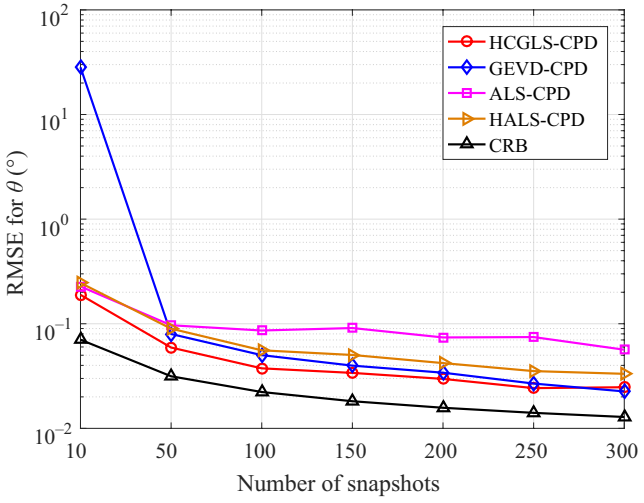

FIGURE 1 DoA RMSE vs K and $L = 4$

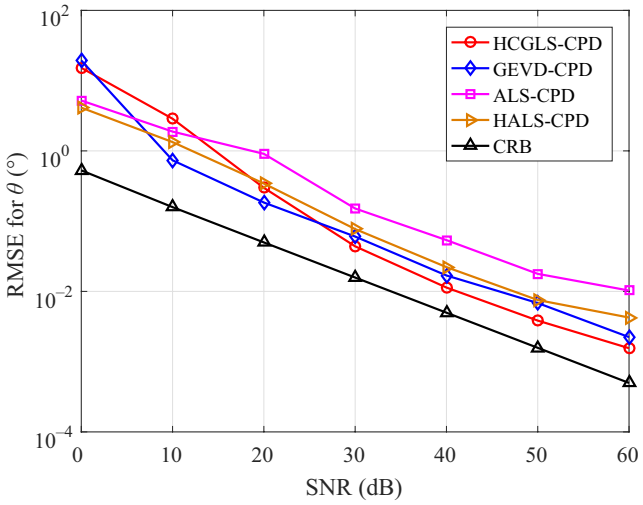

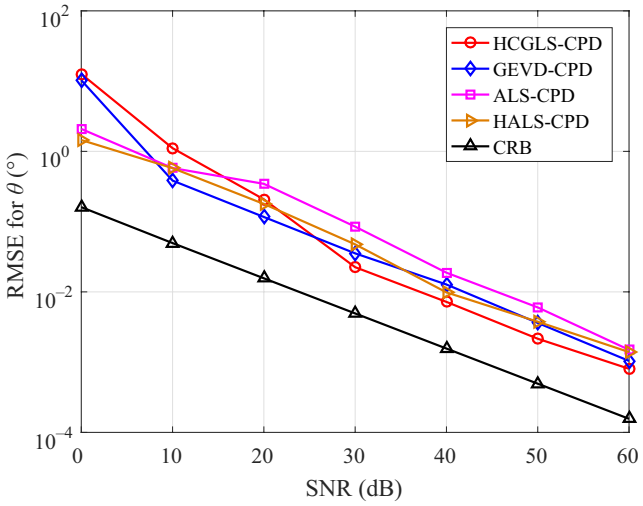

FIGURE 2 DoA RMSE vs SNR for $K = 200$ and various numbers of sensors. (A) $L = 4$, (B) $L = 8$

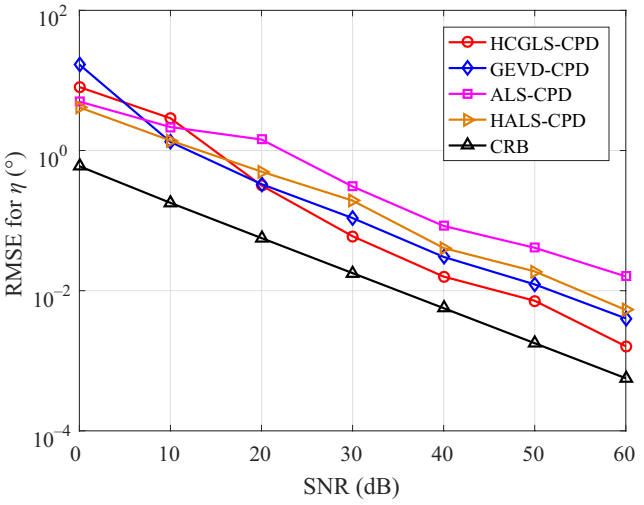

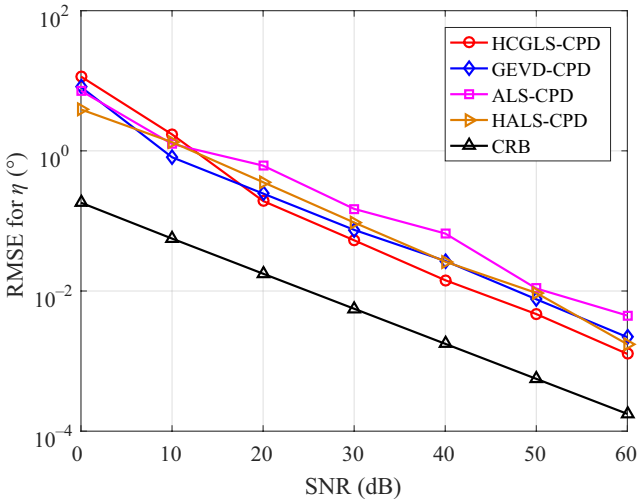

FIGURE 3 Polarization parameter RMSE vs SNR for $K = 200$ and various numbers of sensors. (A) $L = 4$, (B) $L = 8$

be explained by the cumulative error because the polarization parameters were obtained on the premise of DoA estimation.

6 | CONCLUSIONS

This paper proposes a hierarchical CGLS algorithm for the tensor CPD. The proposed algorithm was used to tackle the problem of signal parameter estimation. The procedure of the proposed HCGLS-CPD algorithm was described along with the algebraic method used to estimate the signal parameters. The strength of the proposed HCGLS-CPD algorithm lies in the fact that its convergence and accuracy outperform state-of-the-art algorithms in the extraction of factor matrices. Moreover, the proposed algorithm can more accurately estimate the parameters, particularly when the number of snapshots is relatively small.

ACKNOWLEDGMENTS

This study was supported by the National Natural Science Foundation of China under Grant Nos. 61771404 and 61601372.

CONFLICT OF INTEREST

The authors declare that there is no potential conflict of interest.

AUTHOR CONTRIBUTIONS

LL proposed the framework of the algorithm. LW wrote the simulation code. YW substantially contributed to the writing of the manuscript, and was responsible for the acquisition of funding. JX handled all figures and tables included in the manuscript. ZZ produced the visualizations included in the manuscript. All authors read and approved the final manuscript.

ORCID

Long Liu https://orcid.org/0000-0002-0338-0323
Ling Wang https://orcid.org/0000-0002-6678-7198
Jian Xie https://orcid.org/0000-0001-9654-064X
Yuexian Wang https://orcid.org/0000-0002-3622-6162
Zhaolin Zhang https://orcid.org/0000-0002-9113-4527

REFERENCES

1. R. Schmidt, *Multiple emitter location and signal parameter estimation*, IEEE Trans. Antennas Propag. **34** (1986), no. 3, 276–280.
2. R. Roy and T. Kailath, *ESPRIT-estimation of signal parameters via rotational invariance techniques*, IEEE Trans. Acoust., Speech, Signal Process. **37** (1989), no. 7, 984–995.
3. G. H. Liu et al., *Modified MUSIC algorithm for DOA estimation with Nystrom approximation*, IEEE Sensors J. **16** (2016), no. 12, 4673–4674.
4. W. Suleiman, M. Pesavento, and A. M. Zoubir, *Performance analysis of the decentralized eigendecomposition and ESPRIT algorithm*, IEEE Trans. Signal Process. **64** (2016), no. 9, 2375–2386.
5. S. Y. Liu et al., *Hierarchical principle-based iterative parameter estimation algorithm for dual-frequency signals*, Circuits Syst. Signal Process. **18** (2019), no. 7, 3251–3268.
6. L. Xu and F. Ding, *Recursive least squares and multi-innovation stochastic gradient parameter estimation methods for signal modeling*, Circuits Syst. Signal Process. **36** (2017), no. 4, 1735–1753.
7. L. Xu and F. Ding, *Iterative parameter estimation for signal models based on measured data*, Circuits Syst. Signal Process. **37** (2018), no. 7, 3046–3069.
8. L. Xu, *The parameter estimation algorithms based on the dynamical response measurement data*, Adv. Mech. Eng. **9** (2017), no. 11, 1–12.
9. X. R. Zhang et al., *Adaptive tensorial beamformer based on electromagnetic vector-sensor arrays with coherent interferences*, Multidim. Syst. Sign. Process. **26** (2015), no. 3, 803–821.
10. L. N. Ribeiro, A. L. F. Almeida, and J. C. M. Mota, *Tensor beam-forming for multilinear translation invariant arrays*, in Proc. IEEE Int. Conf. Acoustics, Shanghai, China, 2016, pp. 2966–2970.
11. L. Liu et al., *Robust tensor beamforming for polarization sensitive arrays*, Multidim. Syst. Sign. Process. **30** (2019), 727–748.
12. I. Domanov and L. D. Lathauwer, *Canonical polyadic decomposition of third-order tensors: Relaxed uniqueness conditions and algebraic algorithm*, Linear Algebra Appl. **513** (2017), 342–375.
13. L. Sorber, M. V. Barel, and L. D. Lathauwer, *Optimization-based algorithms for tensor decompositions: canonical polyadic decomposition, decomposition in rank (Lr, Lr, 1) terms, and a new generalization*, SIAM J. Optim. Apr. **23** (2013), no. 2, 695–720.
14. I. Domanov and L. D. Lathauwer, *Canonical polyadic decomposition of third-order tensors: reduction to generalized eigenvalue decomposition*, SIAM J. Matrix Anal. Appl. **35** (2014), no. 3, 636–660.
15. I. Domanov and L. D. Lathauwer, *On the uniqueness of the canonical polyadic decomposition of third-order tensors—part ii: Uniqueness of the overall decomposition, SIAM*, J. Matrix Anal. Appl. **34** (2013), no. 3, 876–903.
16. A. Cichocki et al., *Tensor decompositions for signal processing applications from two-way to multiway component analysis*, IEEE Signal Process. Mag. **32** (2015), no. 2, 145–163.
17. P. Comon and C. Jutten, *Handbook of blind source separation: independent component analysis and separation*, Academic Press **4** (2010).
18. N. D. Sidiropoulos et al., *Tensor decomposition for signal processing and machine learning*, IEEE Trans. Signal Process. **65** (2017), no. 13, 3551–3582.
19. X. J. Guo et al., *A candecomp/parafac perspective on uniqueness of DOA estimation using a vector sensor array*, IEEE Trans. Signal Process. **59** (2011), no. 7, 3475–3481.
20. F. Raimondi et al., *Tensor decomposition exploiting diversity of propagation velocities: Application to localization of icequake events*, Signal Process. **118** (2016), no. 4, 75–88.
21. D. V. D. Lima et al., *Time-delay estimation via CPD-GEVD applied to tensor-based GNSS arrays with errors*, in Proc. IEEE Int. Workshop Computat. Adv. Multi-Sens. Adaptive Process., Curacao, Netherlands, Dec. 2017, pp. 1–5.
22. L. Wang and R. C. D. Lamare, *Constrained adaptive filtering algorithms based on conjugate gradient techniques for beamforming*, IET Signal Process. **4** (2010), no. 6, 686–697.
23. C Jiang, H. Li, and M. Rangaswamy, *On the conjugate gradient matched filter*, IEEE Trans. Signal Process. **60** (2012), no. 5, 2660–2666.
24. M. Zhang, A. Zhang, and Q. Yang, *Robust adaptive beamforming based on conjugate gradient algorithms*, IEEE Trans. Signal Process. **64** (2016), no. 22, 6046–6057.
25. F. Ding, X. G. Liu, and J. Chu, *Gradient-based and least-squares-based iterative algorithms for Hammerstein systems using the hierarchical identification principle*, IET Contr. Theory Appl. **7** (2013), no. 2, 176–184.
26. M. H. Li and X. M. Liu, *The least squares based iterative algorithms for parameter estimation of a bilinear system with autoregressive noise using the data filtering technique*, Signal Process. **147** (2018), 1–20.
27. J. Pan et al., *A filtering based multi-innovation extended stochastic gradient algorithm for multivariable control systems*, Int. J. Contr. Autom. Syst. **15** (2017), no. 3, 1189–1197.
28. F. Ding and X. H. Wang, *Hierarchical stochastic gradient algorithm and its performance analysis for a class of bilinear-in-parameter systems*, Circuits Syst. Signal Process. **36** (2017), no. 4, 1393–1405.
29. L. Xu et al., *Hierarchical parameter estimation for the frequency response based on the dynamical window data*, Int. J. Contr. Autom. Syst. **16** (2018), no. 3, 1756–1764.
30. L. Xu, F. Ding, and Q. M. Zhu, *Hierarchical Newton and least squares iterative estimation algorithm for dynamic systems by transfer functions based on the impulse responses*, Int. J. Syst. Sci. **50** (2019), no. 1, 141–151.
31. X. Zhang et al., *State filtering-based least squares parameter estimation for bilinear systems using the hierarchical identification principle*, IET Contr. Theory Appl. **12** (2018), no. 12, 1704–1713.
32. L. Xu and F. Ding, *Parameter estimation algorithms for dynamical response signals based on the multi-innovation theory and the hierarchical principle*, IET Signal Process. **11** (2017), no. 2, 228–237.
33. L. Xu, *The damping iterative parameter identification method for dynamical systems based on the sine signal measurement*, Signal Process. **120** (2016), 660–667.

AUTHOR BIOGRAPHIES

Long Liu was born in Hebei, China, in 1989. He received his BS and MS degrees in Electronic Engineering from Northwestern Polytechnical University in 2014 and 2017, respectively. Currently, he is pursuing a PhD degree in Northwestern Polytechnical University. His current research interests are array signal processing and radar signal processing, and particularly multidimensional matrices and tensor operation models.

Ling Wang was born in Guizhou, China, in 1978. He received his BS, MS, and PhD degrees from Xidian University, Xi'an, China, in 1999, 2002, and 2004, respectively. From 2004 to 2007, he worked at the Siemens Academy of the wireless communication unit and the Nokia Siemens Networks research center. Since 2007, he has been with the School of Electronics and Information in Northwestern Polytechnical University. His current research interests include B3G/4G mobile communications; vehicle tracking, telemetry, and command (TT&C); anti-jamming for communications and navigation systems; cognitive radio.

Jian Xie was born in Jiangsu, China, in 1986. He received his MS and PhD degrees from the School of Electronic Engineering, Xidian University, in 2012 and 2015, respectively. He is now an associate professor at Northwestern Polytechnical University. His research interests include antenna array processing and radar signal processing.

Yuexian Wang received his BS degree in Electronics and Information Engineering from Northwestern Polytechnical University, China, in 2006, and his MS and PhD degrees in Electrical and Electronic Engineering from The University of Adelaide, Australia, in 2012 and 2015, respectively. From November 2015 to November 2017, he was a postdoctoral fellow at The University of Adelaide. Since February 2018, he has been with the School of Electronics and Information, Northwestern Polytechnical University, China. His current research interests include array signal processing, compressed sensing, tensor decomposition, and their applications to radar, sonar, and wireless communications.

Zhaolin Zhang received his BS, MS, and PhD degrees from Northwestern Polytechnical University, Xi'an, China, in 2000, 2005, and 2012, respectively. Since 2000, he has been teaching at the School of Electronics and Information at Northwestern Polytechnical University, and was promoted to an associate professor. His current research interests include anti-jamming for communications and navigation systems, array signal processing, and multimedia communications.

APPENDIX A

CRAMÉR-RAO LOWER BOUND FOR VECTOR-SENSOR ARRAY

Let us consider the situation described in (4) and establish its matrix form as follows:

$$\mathbf{x}(k)=\mathbf{A}\mathbf{s}(k)+\mathbf{n}(k), \tag{A1}$$

where $\mathbf{A}=[\mathbf{a}(\Psi_1)\ldots\mathbf{a}(\Psi_R)]\in\mathbb{C}^{LJ\times R}$ and $s(k)=[s_1(k)\ldots s_R(k)]^T\in\mathbb{C}^{R\times 1}$. The vector of unknown parameters is expressed as follows:

$$\mathbf{\Psi}=[\Psi_1\ldots\Psi_R]^T, \tag{A2}$$

where Ψ_r represents the unknown parameters vector of the rth source, $r\in[1,\ldots,R]$. It is assumed that matrix $\mathbf{A}$ in (A1) is a column full rank matrix, and the Jacobian $\partial\mathbf{A}/\partial\mathbf{\Psi}$ is also full rank. Furthermore, we set

$$\widetilde{\mathbf{A}}=[\widetilde{\boldsymbol{a}}_1^{(1)}\ldots\widetilde{\boldsymbol{a}}_{q_1}^{(1)}\ldots\widetilde{\boldsymbol{a}}_1^{(R)}\ldots\widetilde{\boldsymbol{a}}_{q_R}^{(R)}], \tag{A3}$$

$$\widetilde{\boldsymbol{a}}_m^{(n)}=\partial\mathbf{a}(\Psi_n)/\partial\Psi_n(m), \tag{A4}$$

where q_r denotes the number of elements in vector Ψ_r. The main objective of this study was to investigate the performance of estimating $\mathbf{\Psi}$ in (A1) from $\mathbf{x}(1),\ldots\mathbf{x}(K)$.

To simplify the expression of the Cramér-Rao lower bound, two intermediate matrices are constructed as follows:

$$\mathbf{U}=\mathbf{R}_{ss}(\mathbf{A}^H\mathbf{A}\mathbf{R}_{ss}+\sigma^2\mathbf{I})^{-1}\mathbf{A}^H\mathbf{A}\mathbf{R}_{ss}, \tag{A5}$$

$$\mathbf{P}=\mathbf{I}-\mathbf{A}(\mathbf{A}^H\mathbf{A})^{-1}\mathbf{A}^H, \tag{A6}$$

where $\mathbf{R}_{ss}$ denotes the covariance of the signal matrix $\mathbf{S}=[S(1)\ldots s(K)]$, σ^2 is the noise variance, and $\mathbf{I}$ denotes the $R\times R$ unit matrix. The Cramér-Rao lower bound of the unbiased estimation of $\mathbf{\Psi}$ is expressed as follows:

$$\mathbf{CRB}(\Psi)=\frac{\sigma^2}{2K}\{\mathrm{Re}[\mathrm{btr}((1\boxtimes\mathbf{U})\boxdot(\widetilde{\mathbf{A}}^H\mathbf{P}\widetilde{\mathbf{A}})^{bT})]\}^{-1}, \quad \text{(A7)}$$

where 1 denotes the $\overline{q}\times\overline{q}$ matrix with all entries equal to one, $\overline{q}=\sum_{r=1}^{R}q_r$. It is assumed that $\mathbf{Q}_{<ij>}$ with dimension $p_i\times p_j$ is the (i, j)th block entry of matrix $\mathbf{Q}$. The block trace operator $\mathrm{btr}(\cdot)$, block transpose operator bT, block Kronecker product $\boxtimes$, and block Hadamard product $\boxdot$ are defined as follows:

Definition A.1. Block trace operator

$$[\mathrm{btr}(\mathbf{Q})]_{ij}=\mathrm{tr}(\mathbf{Q}_{<ij>}).$$

Definition A.2. Block transpose

$$(\mathbf{Q}^{bT})_{<ij>}=\mathbf{Q}_{<ji>}.$$

Definition A.3. Block Kronecker product

$$(\mathbf{Q}_1\boxtimes\mathbf{Q}_2)_{<ij>}=[\mathbf{Q}_1]_{<ij>}\otimes[\mathbf{Q}_2]_{<ij>}.$$

Definition A.4. Block Hadamard product

$$(\mathbf{Q}_1\boxdot\mathbf{Q}_2)_{<ij>}=[\mathbf{Q}_1]_{<ij>}[\mathbf{Q}_2]_{<ij>}.$$

APPENDIX B

HIERARCHICAL ALS-CPD ALGORITHM

Here, we first reshape the rank-R tensor optimization problem (13) into an R rank-1 tensor optimization problem, as follows:

$$\min \| vec(\mathcal{X}_r)-(\mathbf{b}_r\otimes\mathbf{a}_r\otimes\mathbf{I}_K)\|_2, \quad \text{(B1)}$$

where $\mathcal{X}_r=\mathcal{X}-\sum_{r'\neq r}^{R}\mathbf{a}_{r'}\circledcirc\mathbf{b}_{r'}\circledcirc\mathbf{c}_{r'}, r=1, \ldots, R,$ and $r'=1, \ldots, r-1, r+1, \ldots, R$. Then, the vector $\mathbf{a}_r$ is further updated as follows:

$$\mathbf{c}_r=\frac{1}{d_r}(\mathbf{X}_{(1)}(\mathbf{b}_r\otimes\mathbf{a}_r)-\mathbf{C}_{r'}\mathbf{d}_{r'}), \quad \text{(B2)}$$

where the rth entry of vector $\mathbf{d}$ is $d_r=(\mathbf{b}_r^T\mathbf{b}_r)((\mathbf{a}_r^T\mathbf{a}_r))$, $\mathbf{d}_{r'}=[d_1, \ldots, d_{r-1}, d_{r+1}, \ldots, d_R]^T$. Similarly, the components $\mathbf{a}_r$ and $\mathbf{b}_r$ can be expressed as follows:

$$\mathbf{a}_r=\frac{1}{\tilde{d}_r}(\mathbf{X}_{(2)}(\mathbf{c}_r\otimes\mathbf{b}_r)-\mathbf{A}_{r'}\tilde{\mathbf{d}}_{r'}), \quad \text{(B3)}$$

$$\mathbf{b}_r=\frac{1}{\bar{d}_r}(\mathbf{X}_{(3)}(\mathbf{a}_r\otimes\mathbf{c}_r)-\mathbf{B}_{r'}\bar{\mathbf{d}}_{r'}), \quad \text{(B4)}$$

where $\tilde{d}_r=(\mathbf{c}_r^T\mathbf{c}_r)((\mathbf{b}_r^T\mathbf{b}_r))$ and $\bar{d}_r=(\mathbf{a}_r^T\mathbf{a}_r)((\mathbf{c}_r^T\mathbf{c}_r))$. Obviously, the algorithm requires more iterations; therefore, the execution of the CPD process based on the hierarchical ALS algorithm is less efficient.